Anonymous Referee #1:

General comments:

This manuscript used the weather station data and WRF-SLUCM simulations to analyze the links between UHA and CUHI and BUHI across the Suzhou-Wuxi-Changzhou metropolitan area in the YRD, China. The manuscript is well-structured and the logic is easy to read, and the results are interesting. Therefore, I recommend a Minor Revision before publish this manuscript.

RESPONSE: We sincerely thank you for the time and effort you devoted to reviewing this manuscript. We are grateful for your positive feedback and constructive comments on our work. We have addressed them accordingly, which we hope meets with approval. Please find our point-by-point responses below.

Specific comments:

1. Line 16: the authors showed the intensity reaches 0.32°C in Page 8, Line 200. While "…about 0.3°C" is acceptable for in abstract, please ensure consistency or use the more precise value to match the results in the abstract.

RESPONSE: We thank the reviewer for pointing out this inconsistency. We have revised the abstract to ensure consistency as follows:

Lines 15—16 of the revised manuscript in the abstract:

"Under northwesterly flow, daily mean UHA intensities increase from negative values in upwind regions to 0.32 °C downstream"

2. Line 38-41: "Early observations indicated that……show significant heating up to 70 km downwind of the city". This is an interesting comparison. It would be helpful to briefly discuss the reasons. Is it caused by urbanization? Higher sensitivity of model simulation and satellite data? Or any other reasons?

RESPONSE: We thank the reviewer for raising this comparison. Both factors are relevant, and we elaborate on each below.

First, rapid urbanization is a critical factor. The difference in urban size (area and population) between St. Louis in the 1970s and Chicago in recent years is enormous. Larger cities generate larger heat sources, and their influence extends further before thermal anomalies decay to background levels.

Second, there are limitations in the early methodology and spatial scope. Early conclusions relied primarily on aircraft observations, which were limited by flight range,

single observation duration, and fixed flight altitude. Recent research has benefited from advancements in tools and simulation enhancements. For example, the latter study utilizes Lagrange models to track air mass trajectories, providing three-dimensional data covering the entire region.

In addition, factors such as background meteorological conditions (e.g., moderate wind speeds favor the propagation of thermal plumes over longer distances), and the properties of downstream underlying surfaces (e.g., downstream lakes reduce the propagation distance of heat plumes) also affect the propagation of thermal plumes.

We have added a brief discussion in the manuscript as follows:

Lines 39—44 of the revised manuscript in the introduction:

"Under the background of rapid urbanization, the influence of thermal plumes is further enhanced (Moustaoui and Georgescu, 2025). Early observations indicated that urban thermal plumes could extend 10–15 km downwind (Dirks, 1974; Wong and Dirks, 1978), while recent modelling results show significant heating up to 70 km downwind of the city (Cosgrove and Berkelhammer, 2018). Early observational studies were constrained by sparse measurements and primarily captured near-surface thermal characteristics, whereas recent modelling studies can resolve elevated thermal plumes and diagnose their propagation under a wider range of meteorological conditions."

3. Figure 2: the sensitivity experiment was conducted by replacing built-up areas with croplands. I suggest the authors mark the replaced areas in Figure 2c for better reading.

RESPONSE: We appreciate this suggestion and have marked the modified area in Figure 2c accordingly. The areas enclosed by solid black lines and marked with diagonal hatching indicate the regions where the original LULC was modified.

Lines 168—171 of the revised manuscript in Section 2.2.3:

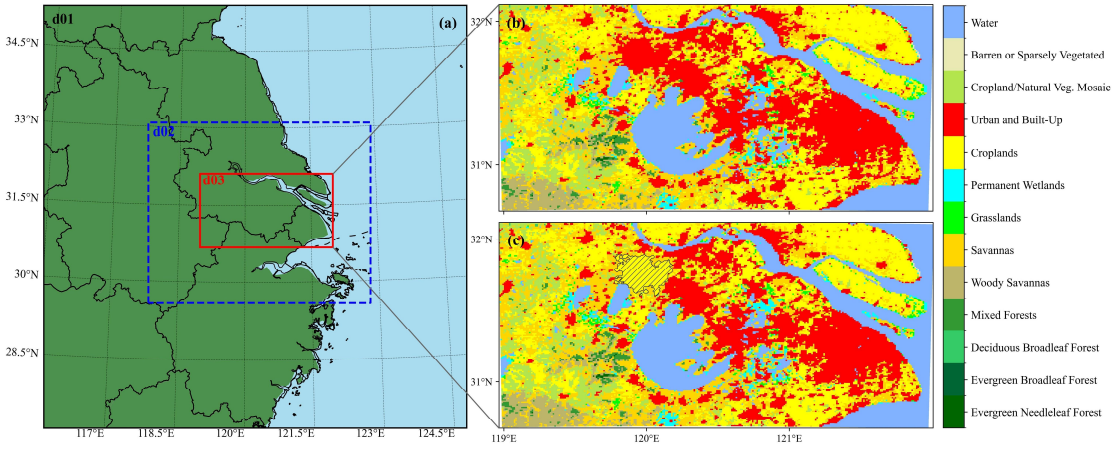

Figure 2. (a) The setup of the nested domain over the study area. Land use and land cover within

the innermost domain for (b) control simulation and (c) sensitivity experiment. In (c), the solid black lines and diagonal hatching represent the areas where the land use/land cover was modified.

4. Section 2.2.3 Model configuration: the research area is a dense metropolitan area, anthropogenic heat flux (AHF) is a major contributor to the initial "heat plume." Can authors clarify in the model description whether a fixed AHF profile was used in the SLUCM or if it was dynamically scaled? This will provide important context for the results.

RESPONSE: We are grateful for this comment, which prompted us to clarify how anthropogenic heat is treated. The original SLUCM run used a default sensible AHF of 50 W m^{-2} scaled by the 24-hour multiplication factors: 0.16 0.13 0.08 0.07 0.08 0.26 0.67 0.99 0.89 0.79 0.74 0.73 0.75 0.76 0.82 0.90 1.00 0.95 0.68 0.61 0.53 0.35 0.21 0.18 (starting at 01 hours local time, no latent AHF).

However, SLUCM systematically overestimates the wind speed in the near-surface layer (Avisar et al., 2021; Sun et al., 2021; Yu et al., 2021), and the default AHF input has uncertainties. In response to this comment, we have replaced SLUCM with the MLUCM BEP+BEM scheme (coupled with a global 1 km spatially continuous urban canopy parameter for the WRF model (Liao et al., 2025)), and the PBL scheme was changed from YSU to MYJ to meet the requirements of BEM.

Consequently, rather than relying on a fixed, prescribed diurnal AHF profile (SLUCM), AHF from buildings is now computed dynamically. Using the default BEM thermodynamic equations, the model dynamically computes the real-time energy required for indoor space heating and the subsequent waste heat rejected into the urban atmosphere. This calculation is driven by the instantaneous outdoor meteorological conditions (e.g., ambient temperature, radiation) and building interior target temperatures. We have supplemented the description of model AHF:

Lines 149—155 of the revised manuscript in Section 2.2.3:

“The spatial features of UHA were evaluated using the Weather Research and Forecasting (WRF) model, version 3.9.1, coupled with a multi-layer urban canopy model (MLUCM). This study utilizes the multi-layer Building Effect Parameterization (BEP) coupled with the Building Energy Model (BEM), and urban canopy parameters were taken from the global 1 km spatially continuous GloUCP dataset (Liao et al., 2025). BEP+BEM can reproduce the intensity and spatiotemporal distribution of UHI (Zhu and Ooka, 2023), and it includes a mature parameterization of the air-conditioning system and of indoor–outdoor heat exchange and accounts for the vertical distribution of AHF (Salamanca

et al., 2010)"

In addition, please see the end of the response for details about the revision of Section 3.3.

5. Figure 4: I suggest adding a vertical dashed line at sunset/sunrise hours in the subplots to help readers better understand the discussion in Line 193-207.

RESPONSE: We thank the reviewer for this helpful suggestion on improving the readability. We have added vertical dashed lines at sunset/sunrise hours in the subplots for Fig. 4 and Fig. 5.

Lines 241—245 in Section 3.1:

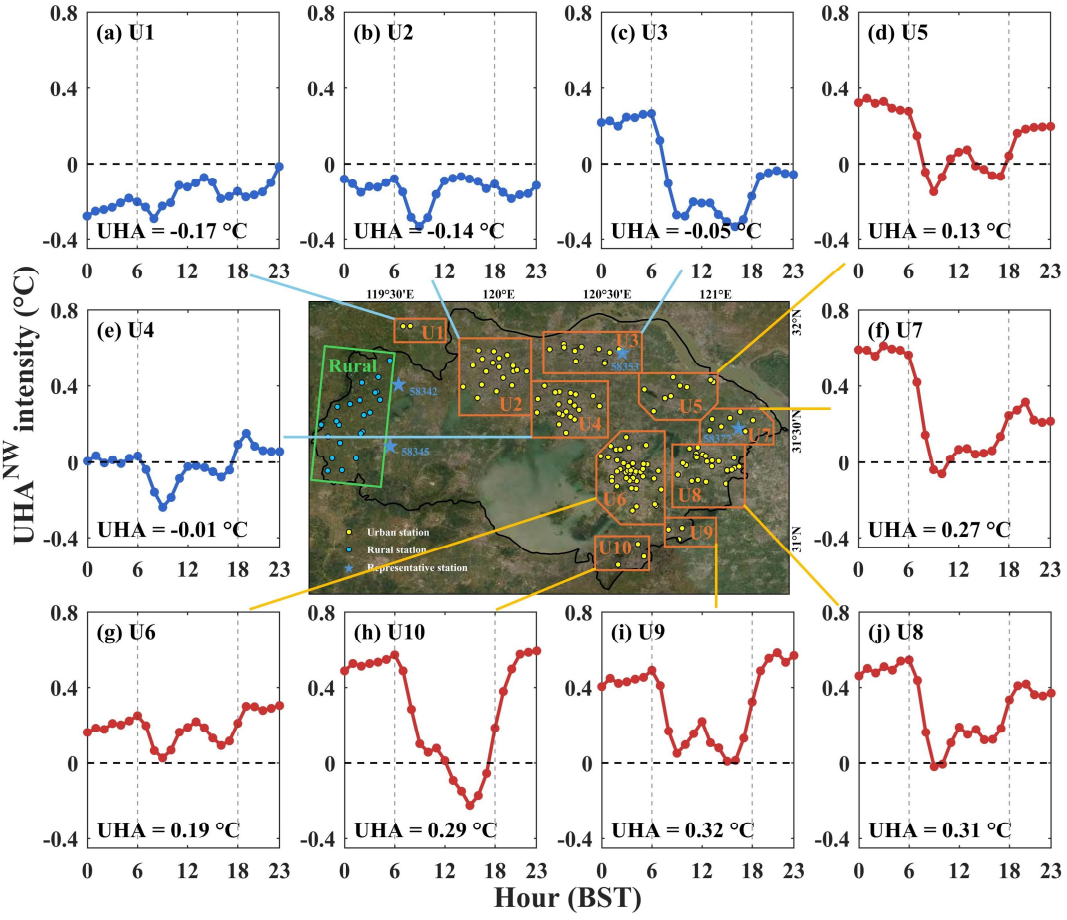

Figure 4. Diurnal variation of hourly UHA intensity across different regions under northwest wind conditions. The numerical values indicate the daily-averaged UHA intensity for each region. Line colours represent the sign of the daily-averaged UHA intensity: red indicates positive values, while blue indicates negative values. Gray vertical lines indicate sunrise/sunset times.

Lines 260—262 in Section 3.1:

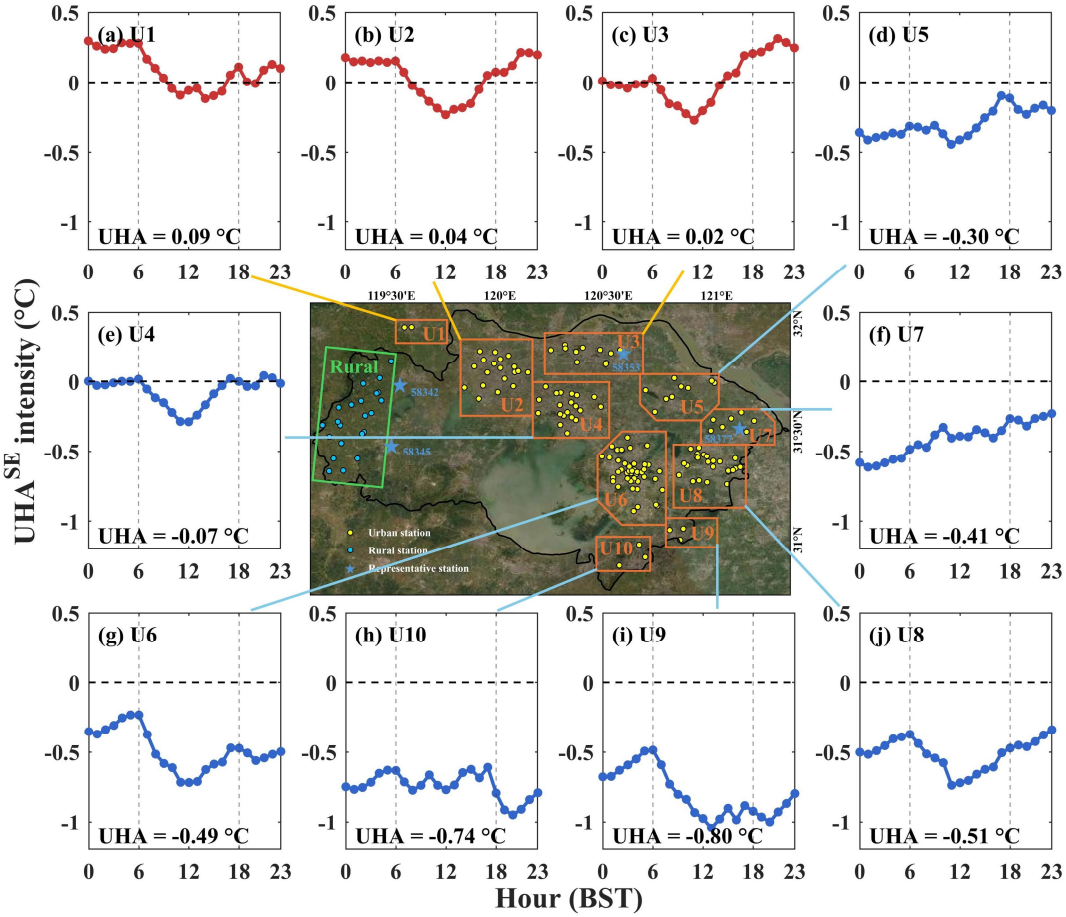

Figure 5. Same as Figure 4, but under southeast wind conditions.

6. Discussion: Given that deep daytime convective boundary layers can reverse the UHA to a cooling effect, do you think your findings would change significantly if the study area included a mega-city with a much deeper PBL, such as Shanghai, in further downwind areas?

RESPONSE: We appreciate this comment regarding the role of a deeper-PBL megacity. The existing conclusions remain unchanged. Please find our response below for details.

Under northwest wind conditions, Shanghai, located downstream of the urban agglomeration (Fig. R1), experiences enhanced heat transport, resulting in a higher average UHA intensity (Fig. R2).

The average PBLH in this study is the regional (ROI) average, not the PBLH of any single city. At the regional scale, a deeper PBL reduces the total advection heat available across the entire region (vertical dilution of heat), thus UHA and PBLH are negatively correlated.

At the local scale, on the one hand, Shanghai receives heat transport from multiple cities, which enhances UHA; on the other hand, Shanghai's higher PBLH vertically dilutes its own heat generation and upstream transport, thus reducing UHA. The final UHA intensity is the

net result of both factors. When upstream heat input is sufficient to outweigh the local vertical dilution, Shanghai exhibits a net positive UHA. This intensified warming may in turn promote further PBL development through enhanced thermal turbulence, although that feedback is not directly diagnosed here.

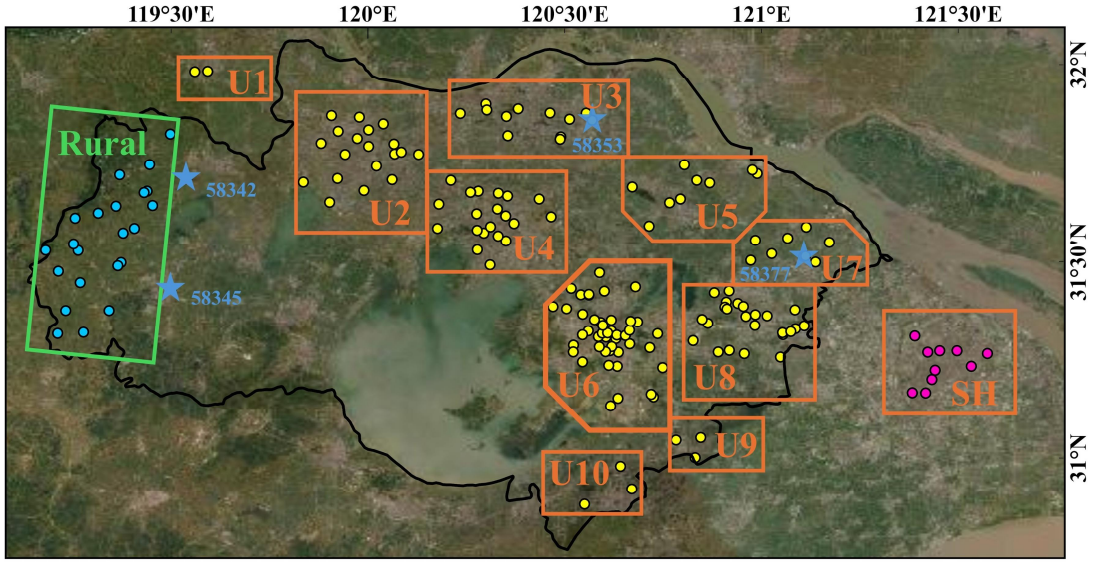

Figure R1. Locations of the automated weather stations, where the yellow and blue circles represent urban and rural stations, respectively, and blue asterisks indicate representative stations of the regional wind field. Note that pink circles represent the urban stations in the Shanghai area.

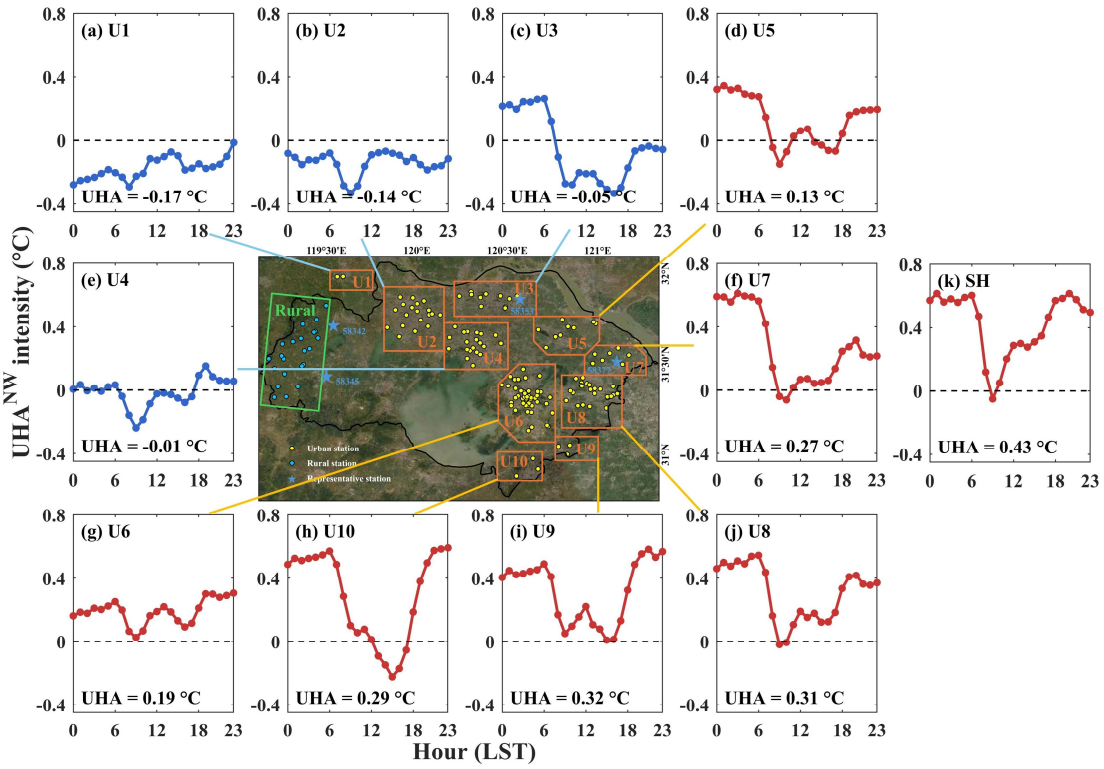

Figure R2. Diurnal variation of hourly UHA intensity across different regions under northwest wind

conditions. The numerical values indicate the daily-averaged UHA intensity for each region. Line colours represent the sign of the daily-averaged UHA intensity: red indicates positive values, while blue indicates negative values. Note that figure R2k represents the Shanghai area.

Furthermore, for numerical simulation, we replaced SLUCM with the MLUCM (BEP+BEM) scheme, drove the urban morphology with the 1 km GloUCP dataset (Liao et al., 2025), and switched the PBL scheme from YSU to MYJ as required by BEM. The entire section 3.3 has been modified based on the new simulation results (as described in question 4). Note that the MYJ scheme results show the phenomenon of heat anomalies reaching the top of the PBL later than YSU, so the displayed times were adjusted. The new results do not affect existing conclusions, and the abstract, data, and methods sections have been modified accordingly.

Line 320—447 in Section 3.3:

"Model performance was evaluated by comparing simulated 2-m air temperature and 10-m wind field of domain 3 against hourly observations from all available meteorological stations within the ROI (Fig. 8). For 2-m air temperature, the RMSE and the Pearson correlation coefficient (R) were 1.80 °C and 0.92 ($p < 0.001$), respectively (Fig 8a). For 10-m wind field, the RMSE for wind direction and wind speed were 34.77° and 2.62 m s^{-1}, respectively (Fig 8b). In addition, the RMSE of PBLH between the model and the dataset (Guo et al., 2024) is 262 m. To provide a more comprehensive validation of the model's performance, we calculated additional statistical metrics for the simulation period. For 2-m air temperature, the Mean Absolute Error (MAE) was 1.29 °C, the Mean Bias (MB) was 0.99 °C (indicating a slight warm bias), and the Index of Agreement (IOA) was 0.93. For 10-m wind speed, the MAE was 2.01 m s^{-1} and the MB was +1.70 m s^{-1} (reflecting a typical overestimation of wind speed by WRF in urban areas due to simplified canopy drag representations (Yu et al., 2021)), with an IOA of 0.71. For the PBLH, the MB compared to the radiosonde-reanalysis merged dataset was –66 m. These quantitative metrics demonstrate that the model captures both the diurnal thermal cycle and the wind-driven transport dynamics with acceptable accuracy, establishing a solid baseline for the sensitivity experiments.

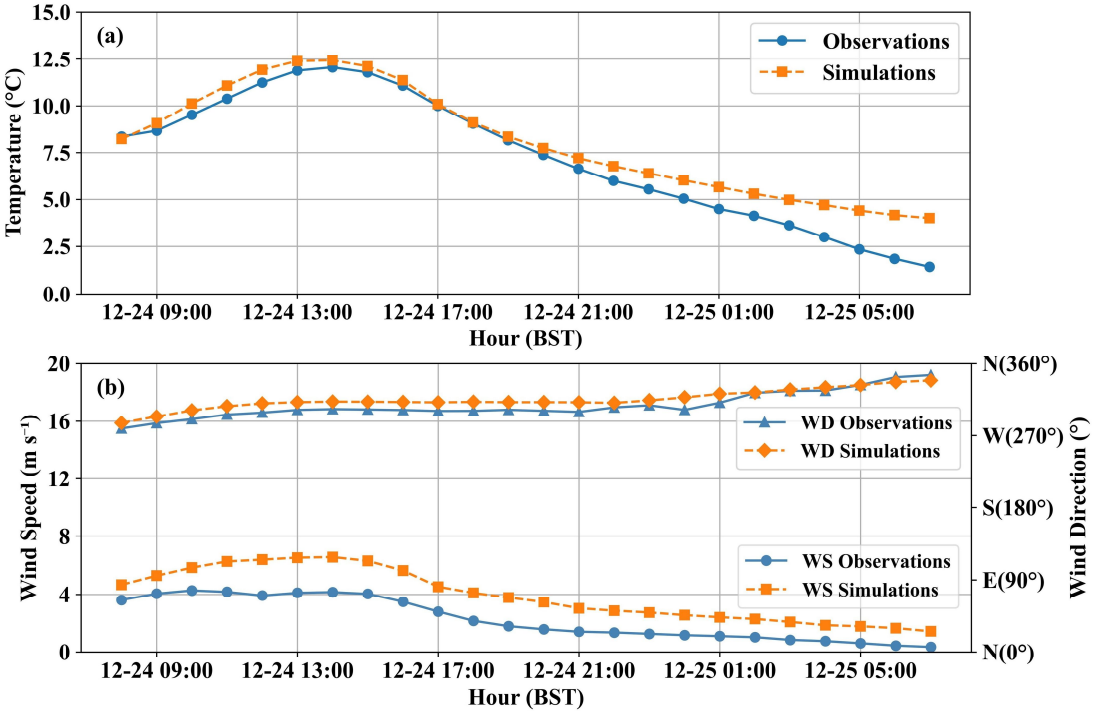

Figure 8. Comparisons of hourly mean (a) 2-meter temperature and (b) 10-meter wind speed (below lines) and wind direction (above lines) from WRF simulations (orange lines) and observations (blue lines) within the ROI.

The observation-based UHA intensity was compared with the WRF-simulated horizontal temperature advection. Taking Wuxi (U4), which lies downwind of Changzhou (U2) under the prevailing northwest wind direction, as an example, the observed daily mean CUHII during the simulation period was 2.24 °C (Fig. 9a). The UHA intensity was negative after sunrise, turned positive around midday, and continued to intensify, reaching a maximum of 3.15 °C at night before declining toward the following morning (Fig. 9b). The daily mean UHA intensity was 1.38 °C, indicating that UHA enhances CUHII under the prevailing wind direction. Fig. 9c shows the difference in horizontal temperature advection between the control and sensitivity experiments (CTRL minus EXP). This difference also exhibited a broadly similar pattern with higher values at night and lower values during the day, with a nighttime peak of approximately 0.45 K/h and a daily mean of 0.18 K/h (Fig. 9c). Overall, the UHA intensity and the horizontal temperature advection showed similar diurnal variations.

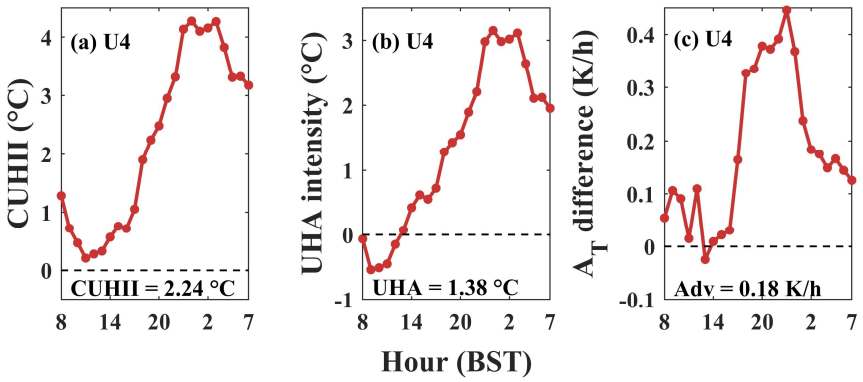

Figure 9. Diurnal variation of hourly (a) CUHII, (b) UHA intensity, and (c) horizontal temperature advection difference between the control simulation and the sensitivity experiment (CTRL minus EXP) over Wuxi (U4) during the simulation period. Annotated values indicate the respective daily means.

"Figure 10 illustrates the spatial distribution of the 2-meter temperature difference between the control and sensitivity simulations (CTRL minus EXP), approximately representing the thermal and dynamic contributions of upstream urbanization in Changzhou to the downstream canopy temperature. During the analysis hours, northwest winds prevailed in domain 3. Influenced by the UHI, Changzhou exhibited a pronounced warming, with positive temperature anomalies of 3.58 °C and 0.42 °C at 22:00 BST and 15:00 BST, respectively. This phenomenon arises from the coupled interplay of thermal and dynamic processes. Thermally, urban materials and anthropogenic heat emissions drive a substantial increase in sensible heat flux. Dynamically, the elevated aerodynamic roughness length of the urban canopy suppresses near-surface wind speeds and ventilation (Oke et al., 2017). Both factors together modulate the local positive temperature anomaly and determine its subsequent advection propagation to downstream regions. The simulations show a diurnal variation in the 2-meter temperature differences. At night (22:00 BST), lower wind speeds were accompanied by a high UHA intensity but with a limited advective distance, and strong warming was concentrated in the short distance downstream of the city (Fig. 10a). In contrast, daytime conditions (15:00 BST) featured higher wind speeds, which were accompanied by lower UHA intensity but a greater thermal influence distance (Fig. 10b). Under the prevailing northwest winds, the U10 region was also affected by the thermal forcing of Taihu Lake in addition to UHA. During winter, Taihu Lake functions as a daytime heat sink and a nighttime heat source relative to the surrounding environment (Fig. S3). Furthermore, Cosgrove and Berkelhammer (2018) utilized a Lagrangian atmospheric transport model to demonstrate that the Chicago urban thermal plume caused significant heating at 100–200 m above ground level, extending up to 70 km downwind. The sensitivity experiments in

this study show that the downstream canopy region was also heated, with the thermal influence beyond 100 km.

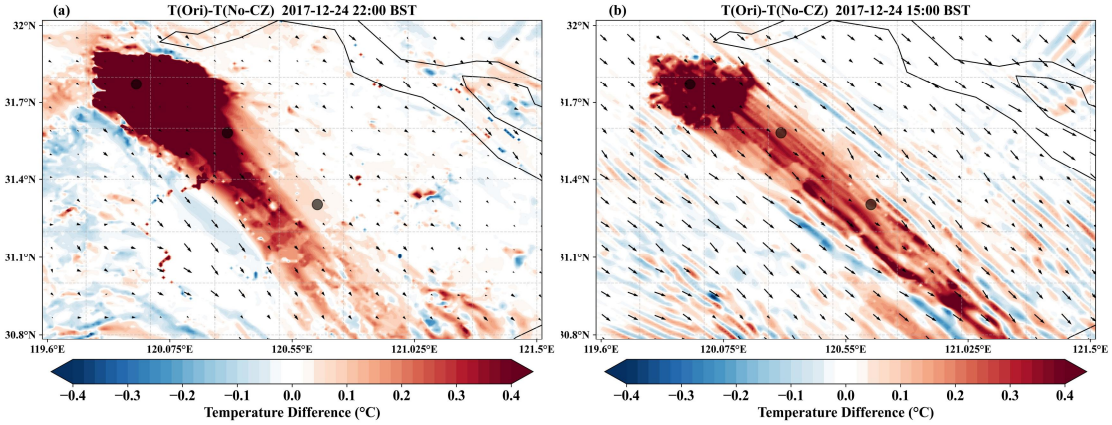

Figure 10. Spatial distribution of the 2-meter temperature difference between the control simulation and the sensitivity experiment (CTRL minus EXP) at (a) 22:00 BST and (b) 15:00 BST. Vector arrows indicate the 10-meter wind field of the CTRL. The three marked locations from northwest to southeast correspond to downtown areas of Changzhou (U2), Wuxi (U4), and Suzhou (U6), respectively.

Vertical cross-sections of potential temperature and wind vector differences between control and sensitivity experiments were analysed (Fig. 11). The cross-section along a northwest-southeast direction spans approximately 114 km (Fig. 11a), encompassing cities from Changzhou (U2) through Wuxi (U4) to Suzhou (U6). Note that the coordinate rotation was applied to the horizontal wind component u to align it with the cross-section direction, with positive values corresponding to northwest winds. For example, significant negative horizontal wind components within Changzhou's near-surface layer are due to the urban rough surface. At night (22:00 BST), the atmospheric stratification is stable, and updrafts and downdrafts induced by the UHI can be observed over urban areas, particularly in Wuxi (see the CTRL results in Figure S4b). Thermal plume was suppressed within the near-surface layer, and substantial heat within Changzhou propagated downstream primarily below 100 m, although the PBLH can reach 750 m (Fig. 11b). Following sunrise, solar shortwave radiation enhanced surface heating and buoyancy-driven turbulence (Zhang et al., 2023), elevating PBLH to approximately 1600 m by afternoon (15:00 BST, Fig. S4c). Compared to nighttime conditions, enhanced ventilation and vertical mixing extended thermal influences throughout the entire PBL depth (Fig. 11c), intensifying the BUHI in Wuxi and Suzhou. As the thermal plume propagates, vertical heat redistribution may occur through turbulent mixing in downstream cities. In addition, the updraft in the downstream area is strengthened, and the vertical circulation in Wuxi during the day may be UHA-enhanced UHI circulation (Fig. 11b-c).

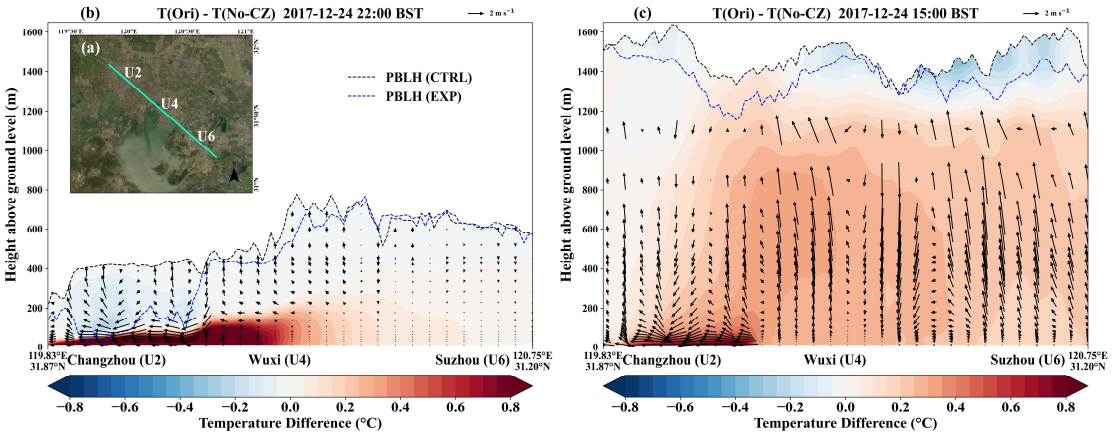

Figure 11. (a) Geographical location of the vertical cross-section. (b, c) Vertical cross-sections of the potential temperature and wind vector differences between the control simulation and the sensitivity experiment (CTRL minus EXP) at (b) 22:00 BST and (c) 15:00 BST. Wind vectors were synthesized by rotating u (along the transect axis) and scaling ω (ω multiplied by 50). The black and blue solid lines denote the PBLH in the CTRL and EXP simulations, respectively.

The sensitivity experiments quantified UHA contributions from a single upstream city. In reality, taking the downstream city of Suzhou as an example, its UHI is influenced by multiple upstream heat sources, including weak UHA transport from distant Changzhou superimposed upon strong UHA contributions from adjacent Wuxi. When the LULCs in upstream Changzhou and Wuxi are simultaneously replaced with croplands in the sensitivity experiment, enhanced cross-city thermal plume superposition and greater PBLH differences were shown (Fig. S5). These results demonstrate that the intensity and spatial structure of UHA are closely related to diurnal boundary layer evolution.

The CUHII differences of the downstream adjacent city Wuxi (U4) were evaluated between two experimental scenarios. Figures 12a show scatter plots of ΔCUHII and both wind speed and PBLH across different hours. Nighttime conditions exhibited a higher ΔCUHII (with a maximum increase of 0.68°C), accompanied by lower wind speed and shallower PBLH (Fig. 12a1–a2); while daytime conditions showed a comparatively lower ΔCUHII (with a minimum increase of 0.17°C), accompanied by higher wind speed and deeper PBLH (Fig. 12a3–a4). The relative increase in CUHII ranged from 8.1% to 60.4%, with the large proportional amplifications occurring during the daytime period. Specifically, the average difference between nighttime and daytime is 0.51 °C (14.2%) and 0.27 °C (18.9%), respectively. At night, ΔCUHII exhibited a non-linear response to increases in wind speed and PBLH, characterized by an initial amplification followed by a decrease (Fig. 12a1–a2). In contrast, daytime ΔCUHII decreased with increasing PBLH, while its correlation with wind speed remained ambiguous (Fig. 12a3–a4). In summary, these sensitivity experiments

provide corroborations for the observational findings, confirming that UHA is regulated by wind speed and PBLH non-linearly.

UHA also contributed to an increase in BUHII in the downstream city of Wuxi (U4, Fig. 12b1–b4). Specifically, ΔBUHII increased by a maximum of 0.40°C and a minimum of 0.11°C, ranging from 4.7% to 41.7%. The average difference between nighttime and daytime is 0.23 °C (7.5%) and 0.23 °C (23.3%), respectively. It should be noted that uncertainties remain in BUHII due to the schemes of PBL and urban canopy (Zhu and Ooka, 2023). In a supplementary sensitivity test utilizing the YSU PBL scheme (Hong et al., 2006) coupled with the SLUCM urban scheme (Fig. S6), while the absolute change in ΔBUHII remains comparable in magnitude, the relative change of ΔBUHII is larger, and its variation characteristics in response to wind speed and PBLH remain uncertain. Because the numerical simulation covered a limited time period, the potential moderating roles of wind speed and PBLH on BUHI were not further examined.

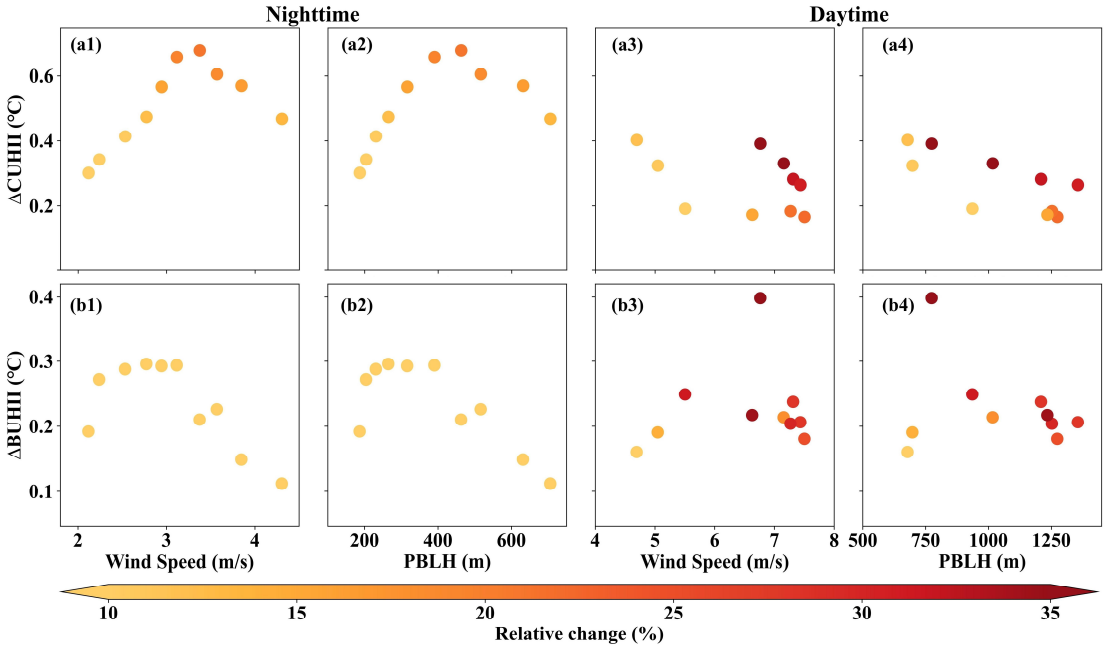

Figure 12. Scatter plots between ΔCUHII and (a1, a3) 10-meter wind speed, and (a2, a4) PBLH between the control simulation and the sensitivity experiment (CTRL minus EXP) over Wuxi (U4) at (a1-a2) nighttime and (a3-a4) daytime. (b1-b4) Same as (a1-a4), but for ΔBUHII. Colours represent the relative change of CUHII or BUHII. Note that only the moment when the northwest wind prevailed in the ROI was reserved.

In addition, the enhancement of downstream UHI (CUHII and BUHII) is primarily contributed to by UHA, though it is not entirely attributable to this mechanism; it is concurrently modulated by other physical processes. For example, advective transport from upstream urban areas can modify local atmospheric conditions (e.g., ambient humidity, stability), which subsequently influence the

thermal environment of the downstream city. Furthermore, changes in the underlying surface will also affect local circulation by thermal (e.g., lake-land breeze circulation) and dynamic (e.g., ventilation) effects, which in turn affect wind and temperature in downstream areas. Ultimately, the increase in downstream UHI is a combined result of multiple processes."

We sincerely appreciate your thorough review and hope these revisions meet with your approval.

Once again, thank you very much for your comments and suggestions.

References (For RESPONSE and newly added references in the manuscript):

Avisar, D., Pelta, R., Chudnovsky, A., and Rostkier-Edelstein, D.: High Resolution WRF Simulations for the Tel-Aviv Metropolitan Area Reveal the Urban Fingerprint in the Sea-Breeze Hodograph, JGR Atmospheres, 126, e2020JD033691, https://doi.org/10.1029/2020JD033691, 2021.

Liao, W., Li, Y., Liu, X., Wang, Y., Che, Y., Shao, L., Chen, G., Yuan, H., Zhang, N., and Chen, F.: GloUCP: a global 1 km spatially continuous urban canopy parameters for the WRF model, Earth Syst. Sci. Data, 17, 2535–2551, https://doi.org/10.5194/essd-17-2535-2025, 2025.

Moustaoui, M. and Georgescu, M.: Winds of Change: The Role of Urban Expansion and Thermal Advection in Driving Phoenix's (AZ) Warming Trends, JGR Atmospheres, 130, e2024JD043166, https://doi.org/10.1029/2024JD043166, 2025.

Salamanca, F., Krpo, A., Martilli, A., and Clappier, A.: A new building energy model coupled with an urban canopy parameterization for urban climate simulations—part I. formulation, verification, and sensitivity analysis of the model, Theor Appl Climatol, 99, 331–344, https://doi.org/10.1007/s00704-009-0142-9, 2010.

Sun, Y., Zhang, N., Miao, S., Kong, F., Zhang, Y., and Li, N.: Urban Morphological Parameters of the Main Cities in China and Their Application in the WRF Model, J Adv Model Earth Syst, 13, e2020MS002382, https://doi.org/10.1029/2020MS002382, 2021.

Yu, M., Chen, X., Yang, J., and Miao, S.: A new perspective on evaluating high-resolution urban climate simulation with urban canopy parameters, Urban Climate, 38, 100919, https://doi.org/10.1016/j.uclim.2021.100919, 2021.

Zhu, D. and Ooka, R.: WRF-based scenario experiment research on urban heat island: A review, Urban Climate, 49, 101512, https://doi.org/10.1016/j.uclim.2023.101512, 2023.